

Reinforcement Learning meets Masked Video Modeling : Trajectory-Guided Adaptive Token Selection

Ayush K. Rai^{*,1}, Kyle Min^{*,2}

Tarun Krishna¹, Feiyan Hu¹, Alan F. Smeaton¹, Noel E. O'Connor¹

¹Insight Research Ireland Centre for Data Analytics, Dublin City University ²Intel Labs, USA

ayush.raai3@mail.dcu.ie kyle.min@intel.com

Abstract

Masked video modeling (MVM) has emerged as a highly effective pre-training strategy for visual foundation models, whereby the model reconstructs masked spatiotemporal tokens using information from visible tokens. However, a key challenge in such approaches lies in selecting an appropriate masking strategy. Previous studies have explored predefined masking techniques, including random and tube-based masking, as well as approaches that leverage key motion priors, optical flow and semantic cues from externally pre-trained models. In this work, we introduce a novel and generalizable Trajectory-Aware Adaptive Token Sampler (TATS), which models the motion dynamics of tokens and can be seamlessly integrated into the masked autoencoder (MAE) framework to select motion-centric tokens in videos. Additionally, we propose a unified training strategy that enables joint optimization of both MAE and TATS from scratch using Proximal Policy Optimization (PPO). We show that our model allows for aggressive masking without compromising performance on the downstream task of action recognition while also ensuring that the pre-training remains memory efficient. Extensive experiments of the proposed approach across four benchmarks, including Something-Something v2, Kinetics-400, UCF101, and HMDB51, demonstrate the effectiveness, transferability, generalization, and efficiency of our work compared to other state-of-the-art methods.

1. Introduction

Self-supervised video representation learning has recently emerged as a prominent area of research due to the generalization capabilities of the learned embeddings. Such representations can be applied to several downstream tasks such as action recognition [22, 60], object detection [2], and segmentation [3] in videos. Due to the scarcity of labeled data, a standard approach in self-supervised learning (SSL)

methods for video understanding involves defining a pretext task. A pretext task can be interpreted as a self-supervised pseudo-objective for pre-training a model. Intuitively, if a model learns to solve a complex task that requires a high-level understanding of its input, then the features learned as a result should generalize well to other tasks.

Inspired by BERT [30] in language modeling, masked modeling in the form of masked autoencoders (MAE) was adopted for images [23, 33, 64] and for videos [14, 52, 59] as a self-supervised pretext task. Masked modeling involves masking a large fraction (between 75-95%) of the input data and then learning to reconstruct or predict the removed content based on the visible information. Although this concept is simple, it has been shown to improve performance [14, 23], generalization [14, 23], data efficiency [52], memory efficiency [4, 14], scalability [23, 59], robustness [24] and to reduce overfitting [17] on downstream tasks.

Several studies have explored different formulations of MAE, focusing on masking portions of input, features, augmenting the masked modeling objective [6, 10, 33, 64, 69, 70, 72]. However, less emphasis has been given to adaptive masking mechanisms that adaptively select space-time patches based on the input. The masking mechanism forms a crucial component of the family of MAE methods, as it is responsible for selecting which information is to be exploited by the encoder and predicted by the decoder.

[23, 70] explored random masking approaches for image patches, blocks, and grids. Though such approaches have shown promise and performance gains on downstream tasks, there still exists a research gap in terms of the masking mechanism being able to adapt to the input. With fixed masking mechanisms, MAEs are unable to exploit the expressivity of transformer-based encoders. In this direction, other contemporary works have investigated different masking strategies for images such as semantically guided masking [33], uniform sampling for pyramid-based vision transformer (ViT) [34] and utilizing mask generators based on object priors [7] and learning easy-to-hard masking through curriculum learning [36].

^{*}Equal contribution

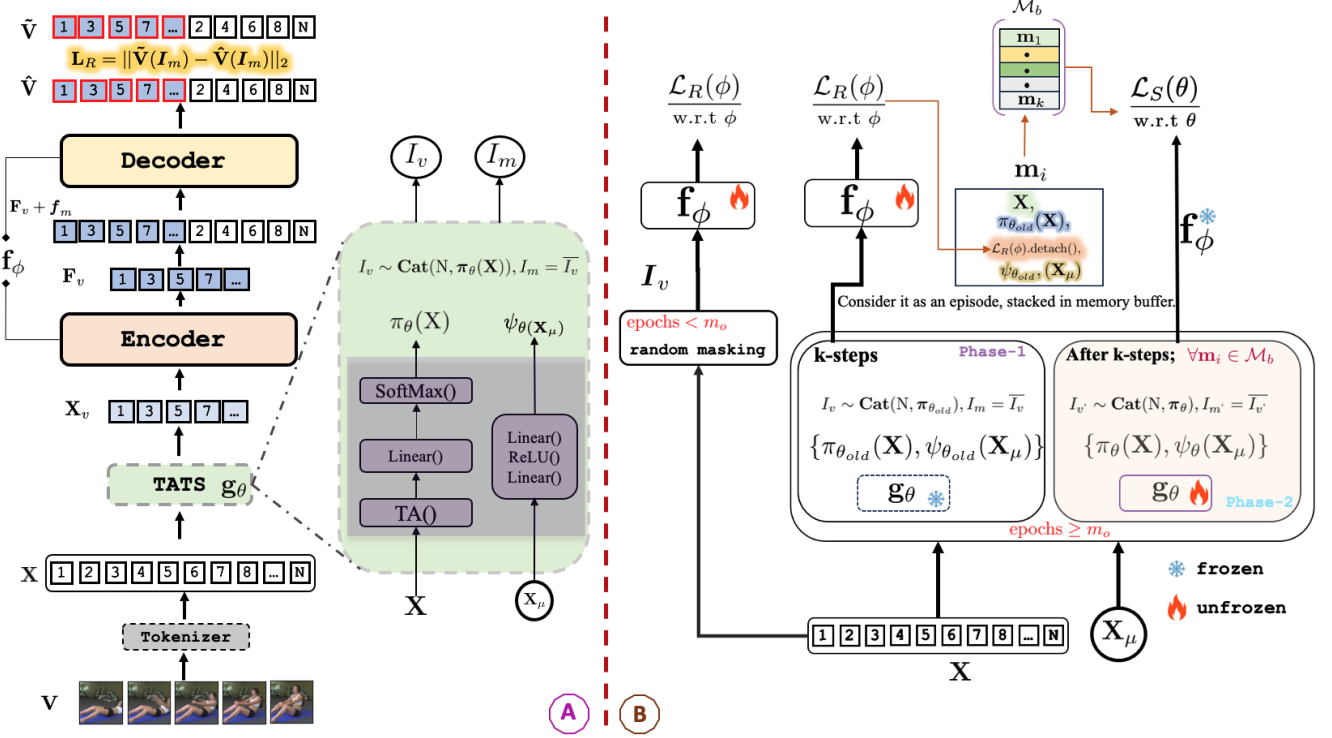


Figure 1. **A** depicts our overall architecture with MAE (f_ϕ) and TATS (g_θ). **B** illustrates the joint training (Algorithm 1) of f_ϕ and g_θ using PPO. Until epoch m_o , standard random space-time masking is applied. Afterward, every k steps, Phase 1 (g_θ frozen, f_ϕ unfrozen) stores old state of g_θ in memory buffer \mathcal{M}_b as episodes, followed by Phase 2 (g_θ unfrozen, f_ϕ frozen), where g_θ is optimized via $L_S(\theta)$. The optimization process then alternates between Phase 1 and Phase 2.

The challenging aspect of MVM is the extra time dimension and high spatiotemporal inductive biases from adjacent frames carrying highly redundant information. This introduces potential information leakage as masked space-time patches can be trivially inferred from spatiotemporal neighborhoods, enabling learning of the shortcuts and less generalizable representations during pre-training. Hence, a substantial amount of compute and memory resources are inefficiently utilized in the prediction of uninformative tokens. On the contrary, such a high level of redundancy can be exploited to aggressively mask space-time tokens with a high mask ratio without compromising the prediction quality of the masked space-time patches.

Several approaches in MVM have utilized frame, tube, and patch-based masking [14, 52, 59], and there is no single universal masking strategy that works for all datasets. VideoMAE [52] achieves the best action classification results on Something-Something v2 (SSv2) [20] with random tube masking while STMAE [14] achieves its best performance on Kinetics-400 (K400) [29] with random space-time patch masking. An explanation for this observation is that not all space-time tokens carry meaningful information, and a fixed masking strategy steers the model’s optimization towards a particular task. Thus, it is crucial to incorporate adaptive

computation in MAEs to dynamically select informative tokens based on the given input and the mask ratio. Previous works such as MGMAE [25] proposed motion-guided masking by extracting the optical flow from pre-trained models, and AdaMAE [4] introduced a token sampler module to select high-activity regions using REINFORCE [67]. In order to exploit unequal information density among patches, we introduce TATS module that learns a video-specific masking strategy from scratch to select space-time patches based on their spatio-temporal motion and trajectory information using Trajectory Attention (TA) [42]. TATS does not rely on any computationally expensive dense optical flow features or semantic cues obtained from external pretrained models like RAFT [51], CLIP [44], or DINOv2 [40].

TATS can be interpreted as a policy agent that models a categorical distribution over the set of input space-time tokens by leveraging their trajectory information and then samples the most relevant tokens based on a predefined mask ratio. However, since training MAE in conjunction with TATS is unstable due to the non-differentiability of the sampling operation, we additionally propose a unified training recipe to train MAE and TATS modules simultaneously using PPO [46] method used in reinforcement learning (RL). Our goal is to incorporate adaptivity into MAEs while pre-

serving their representation quality in terms of generalization and ensuring that the pre-training process remains memory efficient. Overall, our main contributions are:

- We propose a novel and generalizable TATS module that learns to adaptively sample motion-centric tokens for MAE pre-training by modeling their motion trajectories in videos. TATS can be seamlessly integrated into the MAE framework and does not rely on auxiliary modalities like optical flow (RAFT [51]) or external pre-trained models (DINOv2 [40], CLIP [44]) for motion or semantic cues.
- Additionally, we introduce a unified training recipe (Algorithm 1) that facilitates the joint optimization of both MAE and TATS from scratch using PPO [46] to ensure stable convergence during pre-training even with aggressive masking.
- Finally, we conduct a comprehensive evaluation on four benchmark datasets (K400, SSv2, UCF101, HMDB51) for action recognition to demonstrate the effectiveness, generalization, transferability, and efficiency of our work compared to the state-of-the-art methods (Tables 1,2,3).

2. Related Work

2.1. SSL for video representation learning.

SSL has emerged as a promising alternative to the supervised paradigm for pre-training deep models, enabling training on large-scale datasets with enhanced generalization while eliminating the need for labeled annotations. SSL in video primarily focuses on leveraging the temporal dimension for designing tasks such as temporal ordering [16, 32, 38, 58, 65], future prediction [9, 35, 37, 56, 57], spatiotemporal contrast [13, 21, 43, 49], temporal coherence [19, 68] and object motion [1, 41, 62, 63].

2.2. Masked Modeling.

Masked Language Modeling has been universally adopted in natural language understanding, leading to groundbreaking works such as BERT [30]. Several researchers have adopted masked prediction for images/videos through Masked Image Modeling (MIM)/MVM, respectively. MIM/MVM can be interpreted as a generalized Denoising Autoencoder [55] where the masking can be attributed to noise addition.

Generative Pre-training from pixels [8] introduced the task of masked pixel prediction. However, pixel-level prediction demands high computational costs for pre-training and results in inferior performance compared to ConvNets. The notion of dividing an image into visual tokens through patches, as introduced in the ViT [11], enabled the adoption of BERT-style pre-training for visual tokens. BeiT [6] and PeCo[10] are built upon using an offline tokenizer to learn discrete codebooks using VQ-VAE [53] with the goal of reconstructing the original image from randomly masked discrete tokens. iBOT [72] and DALL-E [45] proposed

an online tokenizer based on teacher networks trained via self-distillation. Maskfeat [64] introduced reconstruction of Histogram-of-Oriented-Gradients features for masked-out regions. MAE [23] and SimMIM [70] claimed that directly reconstructing the RGB pixel values performs equivalent to codebook-based methods. [71] proposed a theoretical understanding of the masking mechanism.

MVM techniques have been employed for video pre-training by masking random space-time patches as in STMAE [14], or by utilizing tube masking with a high masking ratio, as in VideoMAE [52, 59]. Other MVM approaches include BEVT [60], Masked Video Distillation [61]. Our method is specifically designed for videos but can be integrated into the MAE framework while maintaining the original reconstruction target and MAE architecture without any modifications.

2.3. Masking Strategies in MIM/MVM.

Many studies have demonstrated that the performance of MAEs and their variants on downstream tasks relies heavily on the choice of masking strategy. SemMAE [33] harnesses iBOT [72] for semantic segmentation and generates semantically aware masks for pre-training. ADIOS [47] introduces a method to jointly learn a masking function and an image encoder through an adversarial objective. AutoMAE [7] avails an adversarially-trained mask generator based on Gumbel-softmax [27] for MIM. CL-MAE [36] uses curriculum learning to generate adaptive masks based on the desired level of complexity (i.e. easy to hard masks). Cluster Masking [66] learns to apply random masking to clusters of image patches, while R-MAE [39] focuses on masking pixels within a specified region. [34] proposed a uniform masking strategy that enables MAE pre-training for Pyramid-based ViTs with locality. AttnMask [28] proposed a distillation-based MIM where masking of the student network is guided by attention maps generated by the teacher network. [69] introduced a method to mask the frequency domain representation of the images using low/high pass filters while [15] constructs a patch association graph using attention maps and addresses the unlabeled part partition problem as a graph cut problem using the Expectation-Maximization algorithm [5] to obtain semantics-based masks.

The masking strategy is a core design choice in MVM, which significantly impacts the information that the network learns during pre-training. MGMAE [25] and MGM [12] introduced motion-guided masking by exploiting a pre-trained lightweight optical flow estimator RAFT [51] and motion vectors stored in the H.264 codec to select space-time patches with rich motion information. EVEREST [26] proposed redundancy robust token selection and an information-intensive frame selection mechanism for pre-training and fine-tuning. MME [50] modifies the pre-training objective from the reconstruction of the appearance content to the reconstruction of the motion trajectory. AdaMAE [4], the work

most closely related to ours, proposed an end-to-end trainable token sampling module that learns to sample space-time patches from high-activity regions using REINFORCE [67]. Our approach draws inspiration from AdaMAE [4], however our *TATS* module selects space-time tokens based on their motion trajectories in videos. Additionally, we propose a novel training recipe that jointly optimizes MAE and *TATS* from scratch using PPO, ensuring stable convergence during pre-training, even with aggressive masking.

3. Method

3.1. Overview of MVM

Here we briefly describe important components of a standard MVM method.

Tokenizer. Consider an input video V of size $T \times C \times H \times W$, where T represents the number of frames, C denotes the input channels and H, W is the height and width of a frame. A *Tokenizer* composed of 3D convolutional layer with kernel K of size (t, C, h, w) , stride S of size (t, h, w) and d output channels is availed to tokenize V into N number of tokens with dimension d indicated as \mathbf{X} , where $N = \frac{T}{t} \times \frac{H}{h} \times \frac{W}{w}$. Positional information is further embedded into the tokens using a fixed 3D periodic positional encoding scheme outlined in [54].

Token Sampler. Based on a specific masking mechanism (tube [52], adaptive [4], random space-time [14]), a set of visible token indices \mathbf{I}_v are sampled from \mathbf{X} for a given mask ratio $\rho \in (0, 1)$ while the remaining indices correspond to the masked Indices \mathbf{I}_m . The choice of masking mechanism is a pivotal design choice of MVM techniques.

Encoder-Decoder. The design of encoder-decoder is usually a variant of VideoMAE [52]. The encoded representation \mathbf{F}_v is learned by feeding the sampled visible tokens \mathbf{X}_v into a vision transformer-based encoder. The learned representations for visible tokens \mathbf{F}_v are concatenated with a fixed learnable representation f_m corresponding to the masked tokens. Subsequently, the positional information is added for both representations in the same order. These combined tokens are then passed through a transformer-based decoder to estimate predictions $\hat{\mathbf{V}}$.

The entire network is trained by reconstruction loss computed between ground-truth and predicted values for the masked tokens.

3.2. Trajectory-Aware Adaptive Token Sampler

We propose *TATS* module (g_θ) that can be easily integrated into the family of MAE (f_ϕ) architectures, can be trained from scratch and learns to sample motion-centric tokens without the use of any external pre-trained models to compute optical flow such as RAFT [51] in MGMAE [25], motion vector in MGM [12] or having motion-specific pre-training objective in MME [50]. In particular, we avail of

TA [42], which captures motion dynamics in a video by learning a probabilistic path of a token between frames. By exclusively sampling motion-centric tokens, *TATS* facilitates the encoder to learn more generic and expressive representations, which is crucial for downstream tasks such as action recognition. The computational overhead of *TATS* is minimal compared to MAE.

Trajectory Attention. In the *TATS* module, we apply TA [42] across space-time tokens, where a trajectory represents the probabilistic path of a token in a video sequence determined by the motion between a pair of frames. A set of query-key-value vectors $\mathbf{q}_{st}, \mathbf{k}_{st}, \mathbf{v}_{st} \in \mathbb{R}^d$ are computed through linear projections (W) for a given space-time token \mathbf{x}_{st} ($\mathbf{x}_{st} \in \mathbf{X}$) corresponding to space-time location st ('reference point') in a video. For \mathbf{q}_{st} , a set of trajectory tokens $\tilde{\mathbf{y}}_{stt'} \in \mathbb{R}^d$ are computed, encapsulating spatially pooled information weighted by the trajectory probability. These trajectory tokens, extend throughout the video sequence and can be represented independently at different time steps t' .

$$\tilde{\mathbf{y}}_{stt'} = \sum_{s'} \mathbf{v}_{s't'} \cdot \frac{\exp\langle \mathbf{q}_{st}, \mathbf{k}_{s't'} \rangle}{\sum_{\bar{s}} \exp\langle \mathbf{q}_{st}, \mathbf{k}_{\bar{s}t'} \rangle}. \quad (1)$$

Here, \exp denotes the exponential function, $\langle \cdot, \cdot \rangle$ represents dot product, and \cdot indicates element-wise multiplication. Next, trajectories are pooled across time to capture intra-frame relationships. The trajectory tokens $\tilde{\mathbf{y}}_{stt'}$ are mapped to a new set of query, key, and value representations, denoted as $\tilde{\mathbf{q}}_{st}, \tilde{\mathbf{k}}_{stt'}, \tilde{\mathbf{v}}_{stt'}$, using the projection matrix \tilde{W} . Now $\tilde{\mathbf{q}}_{st}$ becomes the updated reference query for reference point st . $\tilde{\mathbf{q}}_{st}$ is then utilized to aggregate information across the temporal dimension using 1D attention given by:

$$\mathbf{y}_{st} = \sum_{t'} \tilde{\mathbf{v}}_{stt'} \cdot \frac{\exp\langle \tilde{\mathbf{q}}_{st}, \tilde{\mathbf{k}}_{stt'} \rangle}{\sum_{\bar{t}} \exp\langle \tilde{\mathbf{q}}_{st}, \tilde{\mathbf{k}}_{\bar{s}t} \rangle}. \quad (2)$$

The trajectory information is encoded in \mathbf{y}_{st} . In practice, we employ an approximation of TA (Orthoformer [42]), which has linear complexity in space-time.

The **TATS module** (g_θ) has two branches, one of which processes the input tokens \mathbf{X} by passing them through a block of TA followed by a *Linear* layer, and a *Softmax* activation to compute the probability scores $\pi_\theta(X) \in \mathbb{R}^N$ for all tokens.

$$\mathbf{Z} = \text{TA}(\mathbf{X}); \mathbf{Z} \in \mathbb{R}^{N \times d} \quad (3)$$

$$\pi_\theta(X) = \text{Softmax}(\text{Linear}(\mathbf{Z})) \in \mathbb{R}^N \quad (4)$$

Following AdaMAE [4], these probability scores are utilized to define an N -dimensional categorical distribution over $\pi_\theta(X)$, from which visible token indices are sampled without replacement i.e. $\mathbf{I}_v \sim \text{Categorical}(N, \pi_\theta(X))$. The masked token indices are the complement of visible token indices and are given by $\mathbf{I}_m = \overline{\mathbf{I}_v}$. The number of sampled visible tokens $N_v = N \times (1 - \rho)$ and $\rho \in (0, 1)$ is the

predefined mask ratio. This branch can be interpreted as the actor-network (or policy network), which outputs the probability of relevance for every token. In other words, this output probability can be perceived as policy $\pi_\theta(X)$ representing the likelihood of a token being selected given its token representation X . The second branch processes the mean representation of all the tokens (X_μ) and passes it through a feed-forward network consisting of two linear layers with a ReLU activation $\text{Linear}(1568) \rightarrow \text{ReLU}(\text{Linear}(784)) \rightarrow 1$. This can be interpreted as the value network, which learns to predict the expected reward for the current input tokens X , given a mean state X_μ . We denote the output of the value network as $\psi_\theta(X_\mu)$. This value is used for computing the advantage $A(X, I_m)$ as detailed in the optimization section. Overall, the computation of $TATS(g_\theta)$ can be represented as:

$$\pi_\theta(X), \psi_\theta(X_\mu) = g_\theta(X) \quad (5)$$

The complete architecture is shown in Fig 1.

3.3. Optimization

TATS can be conceptualized as an agent interacting with its environment, represented by the MAE, with the objective of learning an optimal masking strategy that removes redundant tokens while selecting only the most informative and motion-centric ones for encoding, given a mask ratio ρ . The environment provides feedback to *TATS* through a reward, which corresponds to the reconstruction error \mathcal{L}_R [4].

The intuition for this reward is that tokens with low reconstruction errors are easier to reconstruct and thus contain redundant information, whereas motion-centric tokens, which are more challenging to reconstruct, exhibit higher reconstruction error. Consequently, *TATS* must be optimized to prioritize the selection of these motion-centric tokens or tokens with higher reconstruction error. Our optimization strategy is loosely inspired from application of RL [18] in the context of aligning large language model (LLM) outputs with human preferences. A major challenge in this formulation is the simultaneous training of both the agent (*TATS*) and the reward model (*MAE*), differing from conventional LLM approaches where the reward model is typically pre-trained separately based on human-labeled data. The joint optimization process incorporates two distinct losses, i.e. reconstruction loss and the sampling loss, as outlined below.

Reconstruction Loss: To optimize the MAE (characterized by f_ϕ), we compute the mean squared error loss \mathcal{L}_R between the predicted and the normalized ground-truth RGB values of the masked tokens as shown in the following equation:

$$\mathcal{L}_R(\phi) = \frac{1}{N - N_v} \sum_{i \in I_m} \|\tilde{\mathbf{V}}_i - \hat{\mathbf{V}}_i\|_2 \quad (6)$$

where $\hat{\mathbf{V}}$ denotes the predicted tokens from the decoder, $\tilde{\mathbf{V}}$ represents the patch normalized ground-truth RGB values corresponding to the masked tokens.

Sampling Loss. *TATS* (g_θ) is optimized using the sampling loss $\mathcal{L}_S(\theta)$ based on PPO [46]. To jointly train f_ϕ and g_θ from scratch, we propose a unified training approach that alternates between optimizing f_ϕ and g_θ . Initially, our objective is to train f_ϕ up to epoch m_o using random space-time masking, minimizing the reconstruction loss \mathcal{L}_R . This ensures that the MAE learns the task of reconstructing masked tokens, as the reconstruction error would be used as a reward for sampling the most challenging space-time tokens.

Since g_θ is trained using PPO, which requires episodes recorded from a previous state of g_θ . To facilitate this during Phase 1 (after m_o epochs), for every k steps, g_θ is kept frozen while $I_v \sim \text{Categorical}(N, \pi_{\theta_{\text{old}}}(X))$ and f_ϕ is optimized based on $\mathcal{L}_R(\phi)$. Simultaneously, the memory buffer \mathcal{M}_b is updated with recorded episodes in the form of $\{X, \pi_{\theta_{\text{old}}}(I_m|X), \mathcal{L}_R(\phi).detach(), \psi_{\theta_{\text{old}}}(X_\mu)\}$. Here, X represents the tokens, $\pi_{\theta_{\text{old}}}(I_m|X)$ denotes the probability of sampling the masked indices, $\mathcal{L}_R(\phi)$ corresponds to the reconstruction error from f_ϕ , and $\psi_{\theta_{\text{old}}}(X_\mu)$ represents the output of the value network. Using recorded rewards and value estimates, the advantage is computed as $A_{\theta_{\text{old}}}(X, I_m) = \mathcal{L}_R(\phi) - \psi_{\theta_{\text{old}}}(X_\mu)$.

In Phase 2, f_ϕ is frozen while g_θ is unfrozen. Recorded episodes are then sampled from \mathcal{M}_b , and the current state of g_θ is used for computing $\pi_\theta(X)$, $\psi_\theta(X_\mu) = g_\theta(X)$ and $I_{v'} \sim \text{Categorical}(N, \pi_\theta(X))$. Notably, $\mathcal{L}_R(\phi)$ is detached from the computation graph to prevent gradient propagation in MAE during this step. The overall PPO objective used for training g_θ is defined by the following equation.

$$J^{PPO}(\theta) = \mathbb{E} \left[c_1 J^{\text{CLIP}}(\theta) - c_2 (\psi_\theta(X_\mu) - \mathcal{L}_R(\phi))^2 + c_3 \mathbf{H}(X, \pi_\theta)(\cdot) \right] \quad (7)$$

$$J^{\text{CLIP}}(\theta) = \mathbb{E} \left[\min(r(\theta) A_{\theta_{\text{old}}}(X, I_m), \text{clip}(r(\theta), 1 - \epsilon, 1 + \epsilon) A_{\theta_{\text{old}}}(X, I_m)) \right] \quad (8)$$

where $r(\theta) = \frac{\pi_\theta(I_{m'}|X)}{\pi_{\theta_{\text{old}}}(I_m|X)}$ represents the importance sampling ratio, and $\epsilon = 0.2$ is the clipping (clip) threshold. The term $(\psi_\theta(X_\mu) - \mathcal{L}_R(\phi))^2$ serves as the objective for training the value network, representing the error in value estimation. $\mathbf{H}(X, \pi_\theta)(\cdot)$ denotes the entropy term associated with the tokens X and policy π_θ , promoting sufficient exploration. The coefficients c_1, c_2, c_3 balance $J^{\text{CLIP}}(\theta)$ (policy loss), value loss, and entropy term, respectively, in the overall PPO objective. After completing Phase 2, f_ϕ is unfrozen, \mathcal{M}_b is reset, and the algorithm transitions back to Phase 1. This alternating process continues, switching between Phase 1 and Phase 2 iteratively throughout training. Since we want to minimize the sampling loss hence $\mathcal{L}_S(\theta) = -J^{PPO}(\theta)$. AdaMAE [4] utilizes REINFORCE [67] which has high variance, however using PPO [46] improves stability as it uses a

clipped objective $J^{\text{CLIP}}(\theta)$ preventing it from making large updates, therefore balancing exploration and exploitation. Our training recipe is illustrated in Algorithm 1.

Algorithm 1 Unified Training Recipe for joint optimization of MAE and TATS.

Require: Video V , MAE network f_ϕ , TATS module g_θ , mask ratio ρ , memory buffer \mathcal{M}_b , epochs E , Train only MAE epochs m_o , TATS update interval k , Total number of tokens N .

```

1: Initialize MAE  $f_\phi$  and TATS  $g_\theta$ .
2: for  $e = 1$  to  $E$  do
3:   for step, batch in dataloader do
4:     tokenize  $V$  into  $X$  with indices  $\{I_1, I_2, \dots, I_N\}$ .
5:     if  $e \leq m_o$  then  $\triangleright$  Random Space-Time Masking Phase
6:        $I_v \sim$  Random Distribution with  $\rho$ 
7:       optimize  $\mathcal{L}_R = f_\phi(X_v)$  w.r.t.  $\phi$ .
8:     else  $\triangleright$  TATS Training Phase
9:       freeze  $g_\theta$ , compute  $\pi_{\theta_{\text{old}}}(X), \psi_{\theta_{\text{old}}}(X_\mu) = g_\theta(X)$ .
10:       $I_v \sim \text{Categorical}(N, \pi_{\theta_{\text{old}}}(X))$  with  $\rho$ ;  $I_m = \overline{I_v}$ 
11:      optimize  $\mathcal{L}_R(\phi) = f_\phi(X_v)$  w.r.t.  $\phi$ .
12:      episode =  $\{X, \pi_{\theta_{\text{old}}}(I_m|X), \mathcal{L}_R(\phi).detach(), \psi_{\theta_{\text{old}}}(X_\mu)\}$ 
13:       $\mathcal{M}_b.\text{update}(\text{episode})$ 
14:      if step mod  $k = 0$  then  $\triangleright$  TATS Update
15:        freeze  $f_\phi$ , unfreeze  $g_\theta$ .
16:        for episode in  $\mathcal{M}_b$  do
17:          compute  $\pi_\theta(X), \psi_\theta(X_\mu) = g_\theta(X)$ 
18:           $I_{v'} \sim \text{Categorical}(N, \pi_\theta(X))$ ;  $I_{m'} = \overline{I_{v'}}$ 
19:          optimize  $\mathcal{L}_S(\theta) = -J^{\text{PPO}}(\theta)$  w.r.t.  $\theta$ .
20:        end for
21:        unfreeze  $f_\phi$ .
22:         $\mathcal{M}_b.\text{reset}()$ 
23:      end if
24:    end if
25:  end for
26: end for

```

4. Experimental Setup

Datasets. We validate our method on four benchmarks: SSv2 [20], K400 [29], UCF101 [48] and HMDB51 [31].

Implementation Details. We employ the ViT-Base model ($\approx 87\text{M}$ parameters) [11] for our experiments. The input video has the dimension $16 \times 3 \times 224 \times 224$ while the patch size is $2 \times 3 \times 16 \times 16$ (tubelet length = 2), yielding a total of 1568 tokens. Mask ratio ρ takes the value $\{0.85, 0.90, 0.95\}$. Our experiments contain two types of settings:

1. Small Scale Pre-training. For K400 and SSv2, we construct a smaller training data subset by sampling approximately 15% of the training set (equivalent to validation set size), while maintaining a class distribution consistent with the original dataset. Notably, the validation set remains unchanged from the original dataset. The standard train/validation sets for UCF101 and HMDB51 are used. The models have been pre-trained for 400 epochs with a

Table 1. Comparison of fine-tuning result of **Our** model against baselines ([4, 52]) on action recognition task across benchmark datasets and different ρ with top-1/top-5 accuracy as evaluation metric. (\uparrow) / (\downarrow): denotes increase/decrease in performance)

Dataset	Mask Ratio ρ	VideoMAE [52]		AdaMAE [4]		Ours	
		top-1	top-5	top-1	top-5	top-1	top-5
UCF101	0.85	80.36	94.95	83.98	96.37	85.94 (\uparrow)	96.98 (\uparrow)
	0.90	76.64	94.29	82.42	95.84	84.53 (\uparrow)	96.37 (\uparrow)
	0.95	65.86	89.14	80.83	95.26	81.75 (\uparrow)	95.29 (\uparrow)
HMDB51	0.85	40.82	71.61	41.28	73.37	41.60 (\uparrow)	73.31 (\downarrow)
	0.90	36.39	69.73	39.13	72.33	41.28 (\uparrow)	73.76 (\uparrow)
	0.95	33.98	65.36	37.70	70.38	38.67 (\uparrow)	72.01 (\uparrow)
Kinetics-400	0.85	42.26	68.28	38.97	64.68	43.24 (\uparrow)	68.76 (\uparrow)
	0.90	41.79	68.62	39.50	65.70	43.28 (\uparrow)	68.85 (\uparrow)
	0.95	39.73	66.15	39.42	65.14	41.70 (\uparrow)	67.29 (\uparrow)
SSv2	0.85	37.63	66.47	37.92	66.63	39.96 (\uparrow)	68.10 (\uparrow)
	0.90	37.85	66.86	38.10	66.29	40.79 (\uparrow)	69.30 (\uparrow)
	0.95	37.24	65.92	38.38	67.11	40.25 (\uparrow)	68.73 (\uparrow)

batch size of 32 on 8 Nvidia A100 GPUs.

2. Large Scale Pre-training is also conducted on full SSv2, however due to computational constraints, we only pretrain it for 400 epochs and $\rho = 0.95$ on 8 Nvidia A100 GPUs.

Evaluation on action recognition. To assess the effectiveness of the pre-trained encoder, we conduct end-to-end *fine-tuning* for the action recognition task over 100 epochs with the evaluation metric being top-1 and top-5 accuracy. Most of our experiments are conducted in a small-scale setting, while results for large-scale pre-training and fine-tuning are explicitly reported.

Refer to the supplementary material (supp) for additional implementation details. Source code for this work has been released at github.com/rayush7/rl-videomae.

4.1. Results

We perform extensive quantitative and qualitative studies of our approach on the given datasets and compare the performance against [4] and [52] (baselines) respectively. For fair comparison with our method under small-scale pre-training setup, these baselines were also pretrained (finetuned) for 400 (100) epochs on the same subset (K400/SSv2) using their public source code and default configuration. For large scale pre-training results refer to the supp.

Fine-tuning Results. Table 1 presents the top-1 and top-5 accuracy obtained after fine-tuning our method across different mask ratios, $\rho = \{0.85, 0.90, 0.95\}$. Our approach consistently surpasses [4, 52] across all benchmark datasets and mask ratios with the exception of top-5 accuracy on HMDB51 with $\rho = 0.85$, which is marginally less than [4]. Notably, even under an aggressive masking ratio ($\rho = 0.95$), our model demonstrates superior performance compared to these baselines. These results highlight the effectiveness and generalization capability of the proposed TATS module and the training strategy in terms of learning a better representation quality than learnt by [4, 52].

Transferability. Table 2 presents the transfer performance

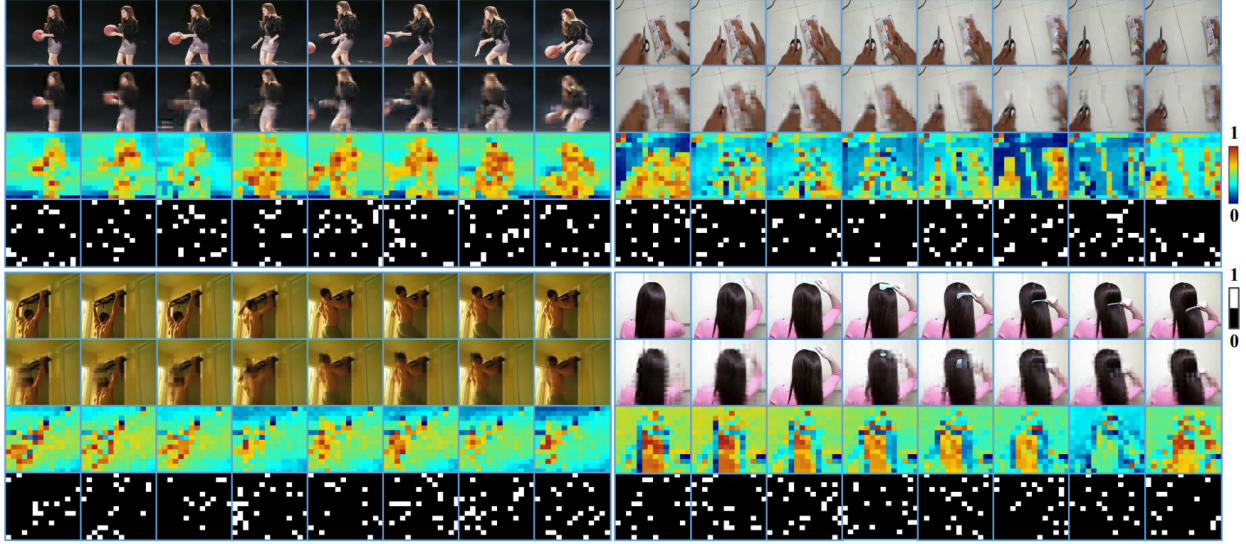


Figure 2. Visualization of adaptive masks learned by *TATS* for $\rho = 0.95$. The figure has four blocks: **top-left** (K400), **top-right** (SSv2), **bottom-left** (UCF101), and **bottom-right** (HMDB51). In each block, the first row shows video frames, the second presents predictions/reconstructions, the third depicts sampling probabilities for space-time tokens, and the fourth displays the learned adaptive binary masks.

of our model on the action recognition task, pre-trained and fine-tuned across different datasets and mask ratio combinations. Our approach achieves better results than [4, 52] across most settings, providing further insight into the strong transferability and generalization of our model.

Qualitative Assessment. We conduct a qualitative analysis by visualizing the learned adaptive binary masks learned by the *TATS* module across the benchmark datasets and different ρ , as shown in Figure 2. We observe that *TATS* learns to sample motion-centric tokens while also undergoing sufficient exploration enabling better generalization. Additionally, we visualize the learned TA across all space-time patches by averaging all heads, as depicted in Figure 3. It is quite evident that our *TATS* module accurately models motion trajectories of the space-time tokens as they evolve over time in the video, thereby enabling the sampling of motion-centric space-time patches. This also validates the formulation of the \mathcal{L}_s and the training recipe to jointly train MAE and *TATS*. Refer to supp for more mask visualizations.

4.2. Ablation Studies

We carry out an ablation study on UCF101 using models pre-trained with $\rho = 0.95$ for 400 epochs and fine-tuned on the action recognition task for 100 epochs. The ablation results are illustrated in Table 3.

1. Effect of Trajectory Attention. In Table 3a, we analyze the effect of integrating TA within the *TATS* module compared to the Multi-Head Self-Attention (MHA). Our findings indicate that TA achieves a top-1 accuracy of 81.75% while utilizing 25.36 GB of memory, outperforming MHA. This

Table 2. Comparison of transfer learning result of **Our** model against [4, 52] on action recognition across benchmark datasets and different ρ with top-1/top-5 accuracy as evaluation metric. (\uparrow) / (\downarrow) / (\rightarrow): denotes increased/decreased/equivalent performance)

Dataset From \rightarrow To	Mask Ratio ρ	VideoMAE [52]		AdaMAE [4]		Ours	
		top-1	top-5	top-1	top-5	top-1	top-5
Kinetics-400 \rightarrow UCF101	0.85	84.91	96.51	85.49	96.93	86.94 (\uparrow)	97.67 (\uparrow)
	0.90	84.41	96.25	84.98	96.48	86.23 (\uparrow)	97.27 (\uparrow)
	0.95	82.40	95.80	84.03	96.50	85.17 (\uparrow)	96.77 (\uparrow)
Kinetics-400 \rightarrow HMDB51	0.85	55.60	82.55	55.79	84.44	60.81 (\uparrow)	84.44 (\rightarrow)
	0.90	56.71	83.07	56.45	82.49	60.42 (\uparrow)	83.59 (\uparrow)
	0.95	53.26	79.75	54.10	81.25	58.14 (\uparrow)	82.62 (\uparrow)
Kinetics-400 \rightarrow SSv2	0.85	36.42	65.50	36.72	65.72	38.39 (\uparrow)	66.47 (\uparrow)
	0.90	35.70	64.46	36.62	65.27	39.46 (\uparrow)	67.25 (\uparrow)
	0.95	34.11	62.64	36.88	65.64	38.13 (\uparrow)	66.48 (\uparrow)
SSv2 \rightarrow UCF101	0.85	84.88	96.91	84.98	96.72	87.16 (\uparrow)	97.38 (\uparrow)
	0.90	83.88	96.75	84.64	97.06	86.81 (\uparrow)	97.51 (\uparrow)
	0.95	82.53	95.90	84.38	96.21	85.14 (\uparrow)	97.11 (\uparrow)
SSv2 \rightarrow HMDB51	0.85	54.82	82.03	55.47	82.81	59.64 (\uparrow)	84.83 (\uparrow)
	0.90	55.92	83.40	55.86	84.31	60.35 (\uparrow)	85.42 (\uparrow)
	0.95	52.41	80.14	54.69	84.18	58.40 (\uparrow)	83.59 (\downarrow)

highlights the efficiency of TA in delivering superior performance with reduced memory consumption. Furthermore, our results also validate that TA effectively captures motion trajectories in a self-supervised manner, without relying on any motion-specific learning objective.

2. Effect of Decoder Depth. Table 3b examines the impact of different decoder depths, specifically the number (#) of transformer blocks in the decoder’s architecture. Our findings show that the best performance is achieved with # Blocks = 1, yielding a top-1 accuracy of 81.75%. This observation aligns with the results observed in [4, 52].

3. Effect of Reconstruction Loss Function. In Table 3d, we examine the effect of the reconstruction objective, specifically comparing L1 and MSE losses. Following the standard

case	ratio	top-1	top-5	memory
MHA	0.95	81.59	95.29	25.37 GB
TA	0.95	81.75	95.42	25.36 GB

(a) **Effect of Trajectory Attention.** Better performance is obtained with TA with marginally less memory usage.

blocks	top-1	top-5	memory
1	81.46	95.07	16.54 GB
2	80.83	95.02	19.48 GB
4	81.75	95.29	25.36 GB
8	79.10	94.68	37.13 GB

(b) **Different decoder depth.** Our method performs best when # of decoder blocks = 4.

method	memory	top-1
VideoMAE [52]	20.94 GB	65.86
AdaMAE [4]	26.17 GB	80.83
Ours	25.36 GB	81.75

(c) **Memory Usage.** Our method uses less memory (pretraining) than [4] while achieving significantly higher performance (finetuning) than [52].

case	top-1	top-5
L1 loss (w norm.)	81.51	95.58
L1 loss (w/o norm.)	81.41	95.02
MSE loss (w norm.)	81.75	95.29
MSE loss (w/o norm.)	81.61	95.14

(d) **Reconstruction Loss function.** The best result is obtained by optimizing MSE loss with local patch normalization.

case	top-1	top-5	memory
TA (# Blocks = 1)	81.75	95.29	25.36 GB
TA (# Blocks = 2)	65.17	88.59	32.18 GB
TA (# Blocks = 3)	67.35	90.20	39.00 GB

(e) **Number of TA blocks in TATS.** Our method performs best when # of TA blocks = 1.

Table 3. Ablation analysis is conducted on the UCF101 dataset using models pre-trained with mask ratio $\rho = 0.95$ for 400 epochs and fine-tuned on action recognition task for 100 epochs. The default choice of our method is highlighted in **gray** color.

approach introduced in VideoMAE [52], we also explore computing these losses (L1/MSE) using both raw pixel values and per-patch normalized pixels. Our results indicate that MSE loss with per-patch normalization achieves the highest top-1 accuracy of 81.75%.

4. Effect of Number of Trajectory Attention Blocks. In Table 3e, we investigate the effect of varying the # of TA blocks in TATS. Our results indicate that the configuration with # TA Blocks = 1 yields the highest top-1 accuracy of 81.75%. As we increase the # TA Blocks, the performance decreases while the memory usage increases.

5. Memory Usage. In Table 3c, we inspect the memory usage of our approach in comparison to AdaMAE [4] and VideoMAE [52]. Our method demonstrates lower memory consumption (pretraining) and better performance (finetuning) than AdaMAE [4]. Although VideoMAE [52] utilizes less memory (pretraining) than our approach, our method significantly outperforms it in terms of top-1 accuracy (finetuning) on UCF101, achieving 81.75% compared to only 65.86% by VideoMAE [52].

5. Conclusions and Discussions

In this work, we propose a novel and generalizable TATS module that enhances MAE pre-training for videos by adaptively selecting motion-centric tokens based on their spatio-temporal motion trajectories. TATS can be integrated into the MAE framework without requiring additional modalities like optical flow (e.g., RAFT [51]) or external pre-trained models such as DINOv2 [40] or CLIP [44] for motion priors or semantic cues. We also introduce a unified training framework (Algorithm 1) that enables the joint optimization of MAE and TATS from scratch using PPO [46], enhancing stability during pre-training even under aggressive masking. Finally, we perform an extensive quantitative, qualitative and ablation assessment (Tables 1,2,3) on benchmark datasets

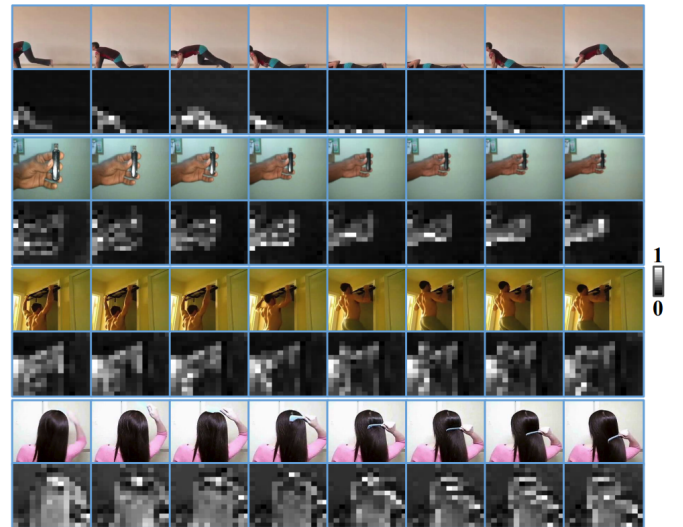


Figure 3. Visualization of the TA learnt by TATS. The figure comprises four blocks : K400, SSv2, UCF101, and HMDB51 in top to bottom order. In each block, the first row shows video frames, the second depicts the trajectory attention on space-time tokens averaged across different heads.

(K400, SSv2, UCF101, HMDB51) for the downstream task of action recognition, showcasing the effectiveness, generalization, transferability, and efficiency of our approach compared to state-of-the-art methods.

Future Work. Our proposed TATS and training recipe does need to be empirically validated on other downstream tasks and extended to other modalities. Furthermore, with the recent resurgence in RL research due to its applications in LLMs, it is important to reconsider strategies that integrate dynamic computation into masked modeling approaches, optimizing them through RL algorithms. We plan to conduct

future studies around these topics. We hope this work can motivate further research in this direction.

6. Acknowledgement

This research is supported by Research Ireland under the Grant Number SFI/12/RC/2289_P2 and Irish Centre for High End Computing (ICHEC).

References

- [1] Pulkit Agrawal, Joao Carreira, and Jitendra Malik. Learning to see by moving. In *Proceedings of the IEEE international conference on computer vision*, pages 37–45, 2015. 3
- [2] Peri Akiva, Jing Huang, Kevin J Liang, Rama Kovvuri, Xingyu Chen, Matt Feiszli, Kristin Dana, and Tal Hassner. Self-supervised object detection from egocentric videos. In *2023 IEEE/CVF International Conference on Computer Vision (ICCV)*, pages 5202–5214, 2023. 1
- [3] Gökay Aydemir, Weidi Xie, and Fatma Güney. Self-supervised Object-centric Learning for Videos. In *Advances in Neural Information Processing Systems*, 2023. 1
- [4] Wele Gedara Chaminda Bandara, Naman Patel, Ali Ghomami, Mehdi Nikkhah, Motilal Agrawal, and Vishal M Patel. Adamae: Adaptive masking for efficient spatiotemporal learning with masked autoencoders. In *Proceedings of the IEEE/CVF Conference on Computer Vision and Pattern Recognition*, pages 14507–14517, 2023. 1, 2, 3, 4, 5, 6, 7, 8
- [5] Arindam Banerjee, Inderjit S Dhillon, Joydeep Ghosh, Suvrit Sra, and Greg Ridgeway. Clustering on the unit hypersphere using von mises-fisher distributions. *Journal of Machine Learning Research*, 6(9), 2005. 3
- [6] Hangbo Bao, Li Dong, Songhao Piao, and Furu Wei. Beit: Bert pre-training of image transformers. In *International Conference on Learning Representations*, 2022. 1, 3
- [7] Haijian Chen, Wendong Zhang, Yunbo Wang, and Xiaokang Yang. Improving masked autoencoders by learning where to mask. In *Chinese Conference on Pattern Recognition and Computer Vision (PRCV)*, pages 377–390. Springer, 2023. 1, 3
- [8] Mark Chen, Alec Radford, Rewon Child, Jeffrey Wu, Heewoo Jun, David Luan, and Ilya Sutskever. Generative pretraining from pixels. In *Proceedings of the 37th International Conference on Machine Learning*, pages 1691–1703. PMLR, 2020. 3
- [9] Ali Diba, Vivek Sharma, Luc Van Gool, and Rainer Stiefelhagen. Dynamonet: Dynamic action and motion network. In *Proceedings of the IEEE/CVF international conference on computer vision*, pages 6192–6201, 2019. 3
- [10] Xiaoyi Dong, Jianmin Bao, Ting Zhang, Dongdong Chen, Weiming Zhang, Lu Yuan, Dong Chen, Fang Wen, Nenghai Yu, and Baining Guo. Peco: Perceptual codebook for bert pre-training of vision transformers. In *Proceedings of the AAAI Conference on Artificial Intelligence*, pages 552–560, 2023. 1, 3
- [11] Alexey Dosovitskiy, Lucas Beyer, Alexander Kolesnikov, Dirk Weissenborn, Xiaohua Zhai, Thomas Unterthiner, Mostafa Dehghani, Matthias Minderer, Georg Heigold, Sylvain Gelly, Jakob Uszkoreit, and Neil Houlsby. An image is worth 16x16 words: Transformers for image recognition at scale. *ICLR*, 2021. 3, 6
- [12] David Fan, Jue Wang, Shuai Liao, Yi Zhu, Vimal Bhat, Hector Santos-Villalobos, Rohith MV, and Xinyu Li. Motion-guided masking for spatiotemporal representation learning. In *Proceedings of the IEEE/CVF International Conference on Computer Vision*, pages 5619–5629, 2023. 3, 4
- [13] Christoph Feichtenhofer, Haoqi Fan, Bo Xiong, Ross Girshick, and Kaiming He. A large-scale study on unsupervised spatiotemporal representation learning. In *Proceedings of the IEEE/CVF conference on computer vision and pattern recognition*, pages 3299–3309, 2021. 3
- [14] Christoph Feichtenhofer, Yanghao Li, Kaiming He, et al. Masked autoencoders as spatiotemporal learners. *Advances in neural information processing systems*, 35:35946–35958, 2022. 1, 2, 3, 4
- [15] Zhanzhou Feng and Shiliang Zhang. Evolved part masking for self-supervised learning. In *Proceedings of the IEEE/CVF Conference on Computer Vision and Pattern Recognition*, pages 10386–10395, 2023. 3
- [16] Basura Fernando, Hakan Bilen, Efstratios Gavves, and Stephen Gould. Self-supervised video representation learning with odd-one-out networks. In *Proceedings of the IEEE conference on computer vision and pattern recognition*, pages 3636–3645, 2017. 3
- [17] Rohit Girdhar, Alaaeldin El-Nouby, Mannat Singh, Kalyan Vasudev Alwala, Armand Joulin, and Ishan Misra. Omnimae: Single model masked pretraining on images and videos. In *Proceedings of the IEEE/CVF Conference on Computer Vision and Pattern Recognition (CVPR)*, pages 10406–10417, 2023. 1
- [18] Yoav Goldberg. Reinforcement learning for language models. URL <https://gist.github.com/yoavg/6bfff0fecdb65950898eba1bb321cfbd81>, 2023. 5
- [19] Ross Goroshin, Joan Bruna, Jonathan Tompson, David Eigen, and Yann LeCun. Unsupervised learning of spatiotemporally coherent metrics. In *Proceedings of the IEEE international conference on computer vision*, pages 4086–4093, 2015. 3
- [20] Raghav Goyal, Samira Ebrahimi Kahou, Vincent Michalski, Joanna Materzynska, Susanne Westphal, Heuna Kim, Valentin Haenel, Ingo Fruend, Peter Yianilos, Moritz Mueller-Freitag, et al. The” something something” video database for learning and evaluating visual common sense. In *Proceedings of the IEEE international conference on computer vision*, pages 5842–5850, 2017. 2, 6, 1
- [21] Tengda Han, Weidi Xie, and Andrew Zisserman. Video representation learning by dense predictive coding. In *Proceedings of the IEEE/CVF international conference on computer vision workshops*, pages 0–0, 2019. 3
- [22] Tengda Han, Weidi Xie, and Andrew Zisserman. Self-supervised co-training for video representation learning. *Advances in neural information processing systems*, 33:5679–5690, 2020. 1
- [23] Kaiming He, Xinlei Chen, Saining Xie, Yanghao Li, Piotr Dollár, and Ross Girshick. Masked autoencoders are scalable

- vision learners. In *Proceedings of the IEEE/CVF conference on computer vision and pattern recognition*, pages 16000–16009, 2022. 1, 3
- [24] Dan Hendrycks, Mantas Mazeika, Saurav Kadavath, and Dawn Song. Using self-supervised learning can improve model robustness and uncertainty. In *Advances in Neural Information Processing Systems*. Curran Associates, Inc., 2019. 1
- [25] Bingkun Huang, Zhiyu Zhao, Guozhen Zhang, Yu Qiao, and Limin Wang. Mgmoe: Motion guided masking for video masked autoencoding. In *Proceedings of the IEEE/CVF International Conference on Computer Vision*, pages 13493–13504, 2023. 2, 3, 4
- [26] Sunil Hwang, Jaehong Yoon, Youngwan Lee, and Sung Ju Hwang. Everest: Efficient masked video autoencoder by removing redundant spatiotemporal tokens. In *International Conference on Machine Learning*, 2024. 3
- [27] Eric Jang, Shixiang Gu, and Ben Poole. Categorical reparameterization with gumbel-softmax. *arXiv preprint arXiv:1611.01144*, 2016. 3
- [28] Ioannis Kakogeorgiou, Spyros Gidaris, Bill Psomas, Yannis Avrithis, Andrei Bursuc, Konstantinos Karantzas, and Nikos Komodakis. What to hide from your students: Attention-guided masked image modeling. In *Computer Vision – ECCV 2022*, pages 300–318, Cham, 2022. Springer Nature Switzerland. 3
- [29] Will Kay, Joao Carreira, Karen Simonyan, Brian Zhang, Chloe Hillier, Sudheendra Vijayanarasimhan, Fabio Viola, Tim Green, Trevor Back, Paul Natsev, et al. The kinetics human action video dataset. *arXiv preprint arXiv:1705.06950*, 2017. 2, 6, 1
- [30] Jacob Devlin Ming-Wei Chang Kenton and Lee Kristina Toutanova. Bert: Pre-training of deep bidirectional transformers for language understanding. In *Proceedings of NAACL-HLT*, pages 4171–4186, 2019. 1, 3
- [31] Hildegard Kuehne, Hueihan Jhuang, Estíbaliz Garrote, Tomaso Poggio, and Thomas Serre. Hmdb: a large video database for human motion recognition. In *2011 International conference on computer vision*, pages 2556–2563. IEEE, 2011. 6, 1
- [32] Hsin-Ying Lee, Jia-Bin Huang, Maneesh Singh, and Ming-Hsuan Yang. Unsupervised representation learning by sorting sequences. In *Proceedings of the IEEE international conference on computer vision*, pages 667–676, 2017. 3
- [33] Gang Li, Heliang Zheng, Daqing Liu, Chaoyue Wang, Bing Su, and Changwen Zheng. Semmae: Semantic-guided masking for learning masked autoencoders. *Advances in Neural Information Processing Systems*, 35:14290–14302, 2022. 1, 3
- [34] Xiang Li, Wenhai Wang, Lingfeng Yang, and Jian Yang. Uniform masking: Enabling mae pre-training for pyramid-based vision transformers with locality. *arXiv preprint arXiv:2205.10063*, 2022. 1, 3
- [35] William Lotter, Gabriel Kreiman, and David Cox. Deep predictive coding networks for video prediction and unsupervised learning. In *International Conference on Learning Representations*, 2017. 3
- [36] Neelu Madan, Nicolae-Cătălin Ristea, Kamal Nasrollahi, Thomas B Moeslund, and Radu Tudor Ionescu. Cl-mae: Curriculum-learned masked autoencoders. In *Proceedings of the IEEE/CVF Winter Conference on Applications of Computer Vision*, pages 2492–2502, 2024. 1, 3
- [37] Michael Mathieu, Camille Couprie, and Yann LeCun. Deep multi-scale video prediction beyond mean square error. In *4th International Conference on Learning Representations, ICLR 2016*, 2016. 3
- [38] Ishan Misra, C Lawrence Zitnick, and Martial Hebert. Shuffle and learn: unsupervised learning using temporal order verification. In *Computer Vision–ECCV 2016: 14th European Conference, Amsterdam, The Netherlands, October 11–14, 2016, Proceedings, Part I 14*, pages 527–544. Springer, 2016. 3
- [39] Duy Kien Nguyen, Yanghao Li, Vaibhav Aggarwal, Martin R. Oswald, Alexander Kirillov, Cees G. M. Snoek, and Xinlei Chen. R-MAE: Regions meet masked autoencoders. In *The Twelfth International Conference on Learning Representations*, 2024. 3
- [40] Maxime Oquab, Timothée Darcet, Theo Moutakanni, Huy V. Vo, Marc Szafraniec, Vasil Khalidov, Pierre Fernandez, Daniel Haziza, Francisco Massa, Alaaeldin El-Nouby, Russell Howes, Po-Yao Huang, Hu Xu, Vasu Sharma, Shang-Wen Li, Wojciech Galuba, Mike Rabbat, Mido Assran, Nicolas Ballas, Gabriel Synnaeve, Ishan Misra, Herve Jegou, Julien Mairal, Patrick Labatut, Armand Joulin, and Piotr Bojanowski. DINOv2: Learning robust visual features without supervision, 2023. 2, 3, 8
- [41] Deepak Pathak, Ross Girshick, Piotr Dollár, Trevor Darrell, and Bharath Hariharan. Learning features by watching objects move. In *Proceedings of the IEEE conference on computer vision and pattern recognition*, pages 2701–2710, 2017. 3
- [42] Mandela Patrick, Dylan Campbell, Yuki Asano, Ishan Misra, Florian Metze, Christoph Feichtenhofer, Andrea Vedaldi, and Joao F Henriques. Keeping your eye on the ball: Trajectory attention in video transformers. *Advances in neural information processing systems*, 34:12493–12506, 2021. 2, 4
- [43] Rui Qian, Tianjian Meng, Boqing Gong, Ming-Hsuan Yang, Huisheng Wang, Serge Belongie, and Yin Cui. Spatiotemporal contrastive video representation learning. In *Proceedings of the IEEE/CVF conference on computer vision and pattern recognition*, pages 6964–6974, 2021. 3
- [44] Alec Radford, Jong Wook Kim, Chris Hallacy, Aditya Ramesh, Gabriel Goh, Sandhini Agarwal, Girish Sastry, Amanda Askell, Pamela Mishkin, Jack Clark, et al. Learning transferable visual models from natural language supervision. In *International conference on machine learning*, pages 8748–8763. PMLR, 2021. 2, 3, 8
- [45] Aditya Ramesh, Mikhail Pavlov, Gabriel Goh, Scott Gray, Chelsea Voss, Alec Radford, Mark Chen, and Ilya Sutskever. Zero-shot text-to-image generation. In *International conference on machine learning*, pages 8821–8831. Pmlr, 2021. 3
- [46] John Schulman, Filip Wolski, Prafulla Dhariwal, Alec Radford, and Oleg Klimov. Proximal policy optimization algorithms. *arXiv preprint arXiv:1707.06347*, 2017. 2, 3, 5, 8
- [47] Yuge Shi, N Siddharth, Philip Torr, and Adam R Kosiorek. Adversarial masking for self-supervised learning. In *Internat-*

- tional Conference on Machine Learning, pages 20026–20040. PMLR, 2022. 3
- [48] Khurram Soomro, Amir Roshan Zamir, and Mubarak Shah. Ucf101: A dataset of 101 human actions classes from videos in the wild. *arXiv preprint arXiv:1212.0402*, 2012. 6, 1
- [49] Chen Sun, Fabien Baradel, Kevin Murphy, and Cordelia Schmid. Learning video representations using contrastive bidirectional transformer. *arXiv preprint arXiv:1906.05743*, 2019. 3
- [50] Xinyu Sun, Peihao Chen, Liangwei Chen, Changhao Li, Thomas H Li, Mingkui Tan, and Chuang Gan. Masked motion encoding for self-supervised video representation learning. In *Proceedings of the IEEE/CVF Conference on Computer Vision and Pattern Recognition*, pages 2235–2245, 2023. 3, 4
- [51] Zachary Teed and Jia Deng. Raft: Recurrent all-pairs field transforms for optical flow. In *Computer Vision—ECCV 2020: 16th European Conference, Glasgow, UK, August 23–28, 2020, Proceedings, Part II 16*, pages 402–419. Springer, 2020. 2, 3, 4, 8
- [52] Zhan Tong, Yibing Song, Jue Wang, and Limin Wang. VideoMAE: Masked autoencoders are data-efficient learners for self-supervised video pre-training. In *Advances in Neural Information Processing Systems*, 2022. 1, 2, 3, 4, 6, 7, 8
- [53] Aaron Van Den Oord, Oriol Vinyals, et al. Neural discrete representation learning. *Advances in neural information processing systems*, 30, 2017. 3
- [54] A Vaswani. Attention is all you need. *Advances in Neural Information Processing Systems*, 2017. 4
- [55] Pascal Vincent, Hugo Larochelle, Yoshua Bengio, and Pierre-Antoine Manzagol. Extracting and composing robust features with denoising autoencoders. In *Proceedings of the 25th International Conference on Machine Learning*, page 1096–1103, New York, NY, USA, 2008. Association for Computing Machinery. 3
- [56] Carl Vondrick, Hamed Pirsiavash, and Antonio Torralba. Anticipating visual representations from unlabeled video. In *Proceedings of the IEEE conference on computer vision and pattern recognition*, pages 98–106, 2016. 3
- [57] Carl Vondrick, Abhinav Shrivastava, Alireza Fathi, Sergio Guadarrama, and Kevin Murphy. Tracking emerges by colorizing videos. In *Proceedings of the European conference on computer vision (ECCV)*, pages 391–408, 2018. 3
- [58] Jiangliu Wang, Jianbo Jiao, Linchao Bao, Shengfeng He, Yunhui Liu, and Wei Liu. Self-supervised spatio-temporal representation learning for videos by predicting motion and appearance statistics. In *Proceedings of the IEEE/CVF conference on computer vision and pattern recognition*, pages 4006–4015, 2019. 3
- [59] Limin Wang, Bingkun Huang, Zhiyu Zhao, Zhan Tong, Yinan He, Yi Wang, Yali Wang, and Yu Qiao. Videomae v2: Scaling video masked autoencoders with dual masking. In *Proceedings of the IEEE/CVF Conference on Computer Vision and Pattern Recognition*, pages 14549–14560, 2023. 1, 2, 3
- [60] Rui Wang, Dongdong Chen, Zuxuan Wu, Yinpeng Chen, Xiyang Dai, Mengchen Liu, Yu-Gang Jiang, Luowei Zhou, and Lu Yuan. Bervt: Bert pretraining of video transformers. In *Proceedings of the IEEE/CVF conference on computer vision and pattern recognition*, pages 14733–14743, 2022. 1, 3
- [61] Rui Wang, Dongdong Chen, Zuxuan Wu, Yinpeng Chen, Xiyang Dai, Mengchen Liu, Lu Yuan, and Yu-Gang Jiang. Masked video distillation: Rethinking masked feature modeling for self-supervised video representation learning. In *Proceedings of the IEEE/CVF conference on computer vision and pattern recognition*, pages 6312–6322, 2023. 3
- [62] Xiaolong Wang and Abhinav Gupta. Unsupervised learning of visual representations using videos. In *Proceedings of the IEEE international conference on computer vision*, pages 2794–2802, 2015. 3
- [63] Xiaolong Wang, Allan Jabri, and Alexei A Efros. Learning correspondence from the cycle-consistency of time. In *Proceedings of the IEEE/CVF conference on computer vision and pattern recognition*, pages 2566–2576, 2019. 3
- [64] Chen Wei, Haoqi Fan, Saining Xie, Chao-Yuan Wu, Alan Yuille, and Christoph Feichtenhofer. Masked feature prediction for self-supervised visual pre-training. In *Proceedings of the IEEE/CVF Conference on Computer Vision and Pattern Recognition*, pages 14668–14678, 2022. 1, 3
- [65] Donglai Wei, Joseph J Lim, Andrew Zisserman, and William T Freeman. Learning and using the arrow of time. In *Proceedings of the IEEE conference on computer vision and pattern recognition*, pages 8052–8060, 2018. 3
- [66] Zihao Wei, Zixuan Pan, and Andrew Owens. Efficient vision-language pre-training by cluster masking. In *Proceedings of the IEEE/CVF Conference on Computer Vision and Pattern Recognition*, pages 26815–26825, 2024. 3
- [67] Ronald J. Williams. Simple statistical gradient-following algorithms for connectionist reinforcement learning. *Machine Learning*, 8:229–256, 1992. 2, 4, 5
- [68] Laurenz Wiskott and Terrence J Sejnowski. Slow feature analysis: Unsupervised learning of invariances. *Neural computation*, 14(4):715–770, 2002. 3
- [69] Jiahao Xie, Wei Li, Xiaohang Zhan, Ziwei Liu, Yew-Soon Ong, and Chen Change Loy. Masked frequency modeling for self-supervised visual pre-training. In *The Eleventh International Conference on Learning Representations*, 2023. 1, 3
- [70] Zhenda Xie, Zheng Zhang, Yue Cao, Yutong Lin, Jianmin Bao, Zhuliang Yao, Qi Dai, and Han Hu. Simmim: A simple framework for masked image modeling. In *Proceedings of the IEEE/CVF conference on computer vision and pattern recognition*, pages 9653–9663, 2022. 1, 3
- [71] Qi Zhang, Yifei Wang, and Yisen Wang. How mask matters: Towards theoretical understandings of masked autoencoders. *Advances in Neural Information Processing Systems*, 35:27127–27139, 2022. 3
- [72] Jinghao Zhou, Chen Wei, Huiyu Wang, Wei Shen, Cihang Xie, Alan Yuille, and Tao Kong. Image BERT pre-training with online tokenizer. In *International Conference on Learning Representations*, 2022. 1, 3

Reinforcement Learning meets Masked Video Modeling : Trajectory-Guided Adaptive Token Selection

Supplementary Material

7. Datasets

Something-Something V2 (SSv2) [20] is a curated video dataset for human action classification, comprising 174 classes and a total of 220,847 videos. Each video depicts a single action with a duration ranging from 2 to 6 seconds. SSv2 is a motion-focused dataset, where temporal relationships are more pronounced compared to other datasets.

Kinetics-400 (K400) [29] is a widely used large-scale video dataset, comprising 400 classes and over 250,000 videos. Each video, approximately 10 seconds in duration, captures a single action.

HMDB51 [31] comprises 51 classes and a total of 6,766 videos. HMDB51 emphasizes appearance information over motion dynamics.

UCF101 [48] comprises 13,320 video clips categorized into 101 classes. These classes span five activity types: body motion, human-to-human interaction, human-to-object interaction, musical instrument performance, and sports.

8. Additional Implementation Details

8.1. Data Preprocessing

Our data processing pipeline closely follows AdaMAE [4] for pre-training. We extract 16 frames of dimension 224×224 from the videos, using a temporal stride of 4 (K400) and 2 (HMDB51/UCF101/SSv2), with the starting frame randomly selected [14]. During pre-training, we apply data augmentation techniques, including random resized cropping

Table 4. Hyperparameter setting for pre-training across all benchmark datasets.

Configuration	Value
Learning rate for $g_\theta - lp$	1.5e-6
Epochs to train f_ϕ only - m_o	10
Steps to train f_ϕ and record g_θ episodes - k	1
Softmax Temperature	1
Policy loss coefficient - c_1	1e-4
Value loss coefficient - c_2	1e-4
Entropy coefficient - c_3	1e-4
Optimizer	AdamW
Optimizer betas	0.9, 0.95
Batch size	32
Base learning rate	1.5e-4
Learning rate schedule	cosine decay
Warmup epochs	40
Augmentation	MultiScaleCrop

Table 5. Hyperparameter (m_o, k) tuning for pre-training, evaluated based on reconstruction error on UCF101 and HMDB51. Same configuration is adopted for SSv2 and K400 as in UCF101.

(m_o, k)	UCF101	HMDB51
(0, 1)	0.5211	0.8051
(1, 1)	0.5205	0.8195
(5, 1)	0.5304	0.8535
(10, 1)	0.5135	0.8278
(25, 1)	0.5269	0.8987
(100, 1)	0.6662	0.9291
(50, 5)	0.7735	0.9772
(50, 10)	0.8149	0.9776
(50, 25)	0.9201	-

in the spatial domain, random scaling within the range $\in [0.5, 1]$, and random horizontal flipping [14].

8.2. Hyper-parameter Setting

Pre-training. The hyperparameter configurations used during the pre-training phase across all benchmark datasets are presented in Table 4. For (m_o, k) , hyperparameter tuning is conducted on the UCF101 and HMDB51 datasets (Table 5), and the configuration that minimizes the reconstruction error is selected. Similarly we also perform hyperparameter tuning for coefficients (c_1, c_2, c_3) in Table 6 during pretraining on UCF101 and observe that (1e-4, 1e-4, 1e-4) minimizes the reconstruction error. Empirical observations indicate that the optimal configuration for UCF101 also performs effectively on subset of K400 and SSv2 (small scale pre-training setup). It is to be noted that we use reconstruction loss for tuning these hyper-parameters because behaviour of reconstruction loss during pretraining is more interpretable in terms of convergence than the sampling loss.

Fine-tuning. The hyperparameter setting for end-to-end fine-tuning on the downstream task of action recognition across all benchmarks is summarized in Table 7.

8.3. Encoder-Decoder Architecture

We adopt an asymmetric encoder-decoder architecture [4] for self-supervised pre-training and augment it with TATS module and only keep the encoder during the fine-tuning. In particular, the design of the encoder-decoder is based on 16-frame vanilla ViT-Base architecture. Table 8 provides an overview of the encoder-decoder architecture utilized in our framework.

Table 6. Hyperparameter (c_1, c_2, c_3) tuning for pre-training, evaluated based on reconstruction error on UCF101. Same configuration is adopted for SSv2, K400 and HMDB51. (m_o, k) are fixed as (10, 1)

(c_1, c_2, c_3)	UCF101
(1e-4, 1e-3, 1e-3)	0.5188
(1e-4, 1e-3, 1e-4)	0.5167
(1e-4, 1e-4, 1e-3)	0.5246
(1e-3, 1e-4, 1e-4)	0.8482
(1e-4, 1e-4, 1e-4)	0.5135
(1e-5, 1e-4, 1e-4)	0.5239
(1e-3, 1e-3, 1e-4)	0.5215
(1e-3, 1e-3, 1e-4)	0.7869
(1e-5, 1e-5, 1e-5)	0.5173

Table 7. Hyperparameter setting for end-to-end fine-tuning for all benchmark datasets.

Configuration	Value
Optimizer	AdamW
Optimizer Betas	{0.9, 0.999}
Batch size	8
Weight Decay	5e-2
Base Learning Rate	1e-3
Learning Rate Schedule	cosine decay
Layer-wise learning rate decay	0.75
Warmup epochs	5
RandAug	9, 0.5
Label Smoothing	0.1
Mixup	0.8
DropPath	0.1
# Temporal Clips	5 (k400), 2 (ssv2/hmdb/ucf)
# Spatial Crops	3

9. Large Scale Pre-training Results

We conduct pre-training (400 epochs) and finetuning (100 epochs) of our model on full SSv2 [20] dataset for $\rho = 0.95$ on 8 Nvidia A100 GPUs. In order to ensure fairness in comparison, we also pre-train (400 epochs) and finetune (100 epochs) both baselines VideoMAE [52] and AdaMAE [4] on full SSv2 for $\rho = 0.95$ with the same GPU setup using their public source code and default configuration.

Table 9 presents the top-1 and top-5 accuracy obtained in this experiment. We observe that our approach outperforms both the baselines under aggressive masking setting even for large scale experiments. This highlights the effectiveness and generalization capability of the proposed *TATS* module and the training strategy in terms of learning a better feature quality than learnt by [4, 52].

Due to the availability of limited computational resources, our experiments in this setup is limited.

Table 8. Encoder-Decoder architecture based on AdaMAE [4]. TATS : Trajectory Aware Adaptive Token Sampler. MHA : Multi-Head Self-Attention

Stage	ViT-Base	Output shape
Input Video	stride $4 \times 1 \times 1$ for K400 stride $2 \times 1 \times 1$ for ssv2/ucf/hmdb	$3 \times 16 \times 224 \times 224$
Tokenization	stride $2 \times 16 \times 16$ emb. dim 768 kernel size $2 \times 16 \times 16$	1568×768
Masking	TATS Masking mask ratio ρ	$[(1 - \rho) \times 1568] \times 768$
Encoder	$[MHA(768)] \times 12$	$[(1 - \rho) \times 1568] \times 768$
Projection	<i>MHA</i> (384) concat masked tokens	1568×384
Decoder	$[MHA(384)] \times 4$	$[(1 - \rho) \times 1568] \times 384$
Projector	<i>MLP</i> (1536)	1568×1536
Reshaping	from 1536 to $3 \times 2 \times 16 \times 16$	$3 \times 16 \times 224 \times 224$

Table 9. **Large Scale Pre-training and Finetuning Results.**

Comparison of fine-tuning result of **Our** model against baselines ([4, 52]) on action recognition task for full SSv2 and $\rho = 0.95$ with top-1/top-5 accuracy as evaluation metric. (\uparrow) : denotes increase in performance)

Method	top-1	top-5
VideoMAE [52] $_{\rho=95\%}$	59.38	84.17
AdaMAE [4] $_{\rho=95\%}$	63.06	85.89
Ours $_{\rho=95\%}$	65.82 (\uparrow)	88.50 (\uparrow)

10. Mask Visualization

Here we show visualizations **adaptive sampling learned by our *TATS* module** across benchmark dataset for different mask ratios $\rho = \{0.95, 0.9, 0.85\}$ in Figure 4, 5, 6, 7, 8, 9, 10, 11, 12, 13, 14, 15.

In all of these Figures, first row represents input video frames, the second row depicts the prediction/reconstruction, the third row shows the reconstruction error, the fourth row represents the probability of sampling the space-time patch, fifth row shows the **adaptive masks learned by *TATS***. The last row depicts the binary masks learned by **AdaMAE** [4] for comparison.

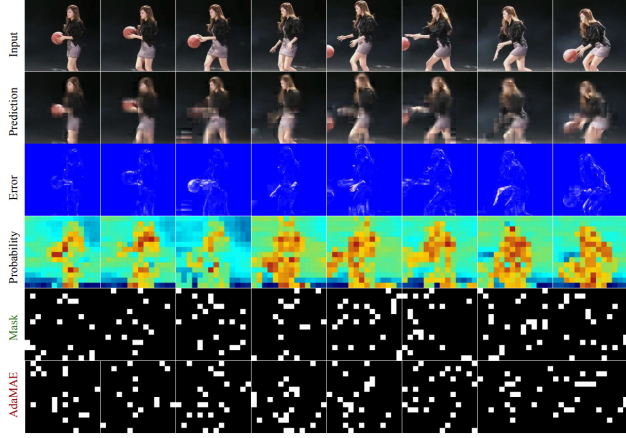


Figure 4. Sample Visualization of a Kinetics 400 video with **adaptive sampling using TATS** with mask ratio $\rho = 0.95$. Compared with **AdaMAE** [4] masks.

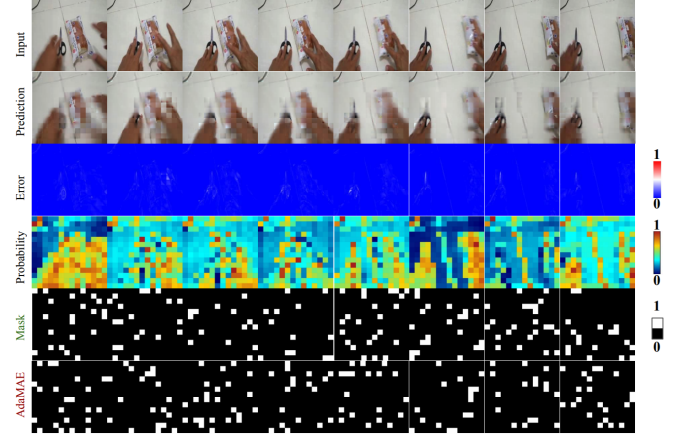


Figure 7. Sample Visualization of a SSv2 video with **adaptive sampling using TATS** with mask ratio $\rho = 0.95$. Compared with **AdaMAE** [4] masks.

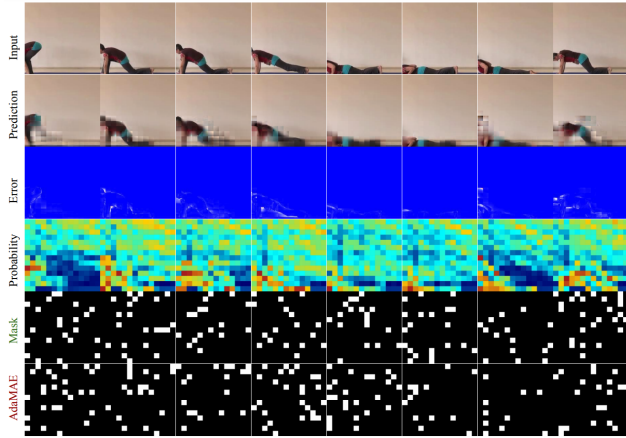


Figure 5. Sample Visualization of a Kinetics 400 video with **adaptive sampling using TATS** with mask ratio $\rho = 0.9$. Compared with **AdaMAE** [4] masks.

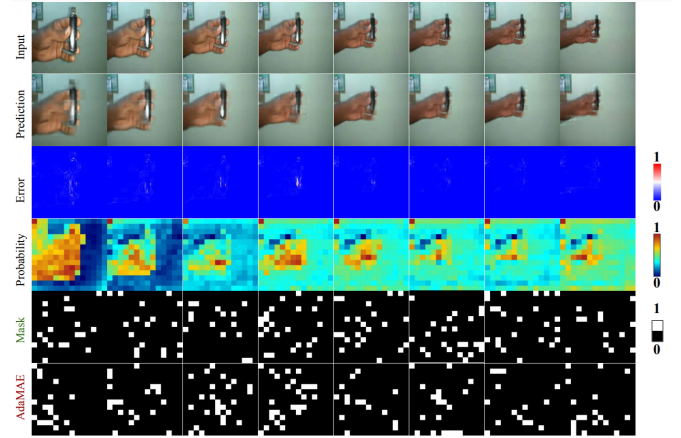


Figure 8. Sample Visualization of a SSv2 video with **adaptive sampling using TATS** with mask ratio $\rho = 0.9$. Compared with **AdaMAE** [4] masks.

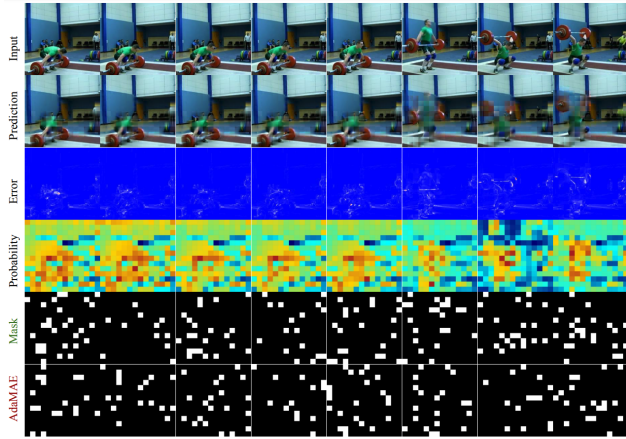


Figure 6. Sample Visualization of a Kinetics 400 video with **adaptive sampling using TATS** with mask ratio $\rho = 0.85$. Compared with **AdaMAE** [4] masks.

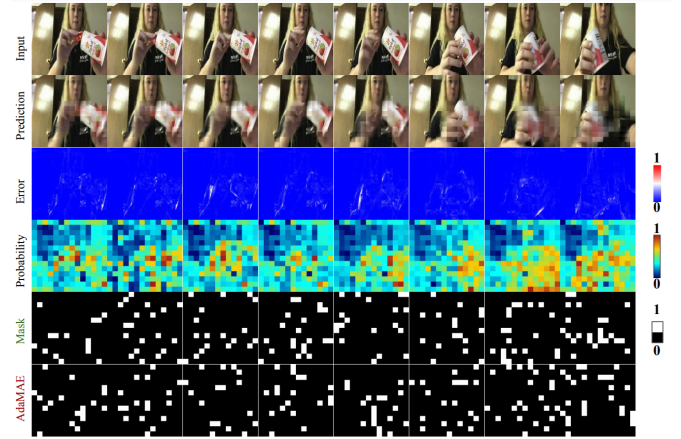


Figure 9. Sample Visualization of a SSv2 video with **adaptive sampling using TATS** with mask ratio $\rho = 0.85$. Compared with **AdaMAE** [4] masks.

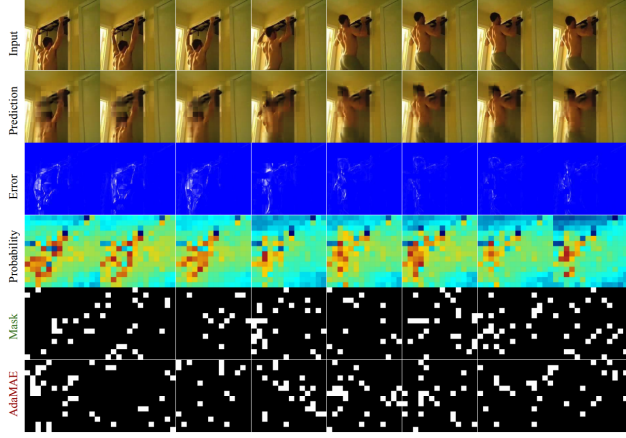


Figure 10. Sample Visualization of a UCF101 video with **adaptive sampling using TATS** with mask ratio $\rho = 0.95$. Compared with **AdaMAE [4]** masks.

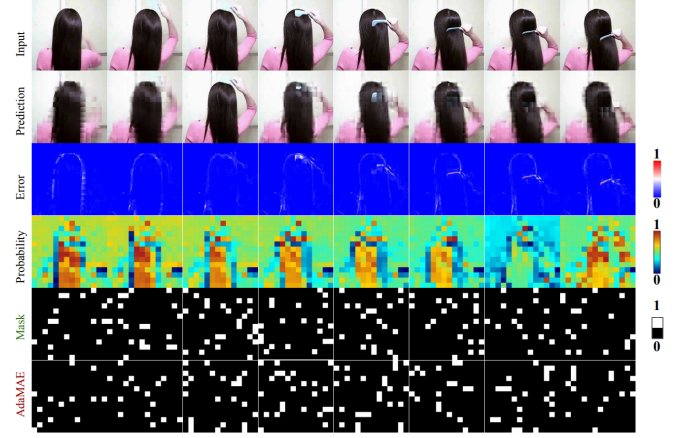


Figure 13. Sample Visualization of a HMDB51 video with **adaptive sampling using TATS** with mask ratio $\rho = 0.95$. Compared with **AdaMAE [4]** masks.

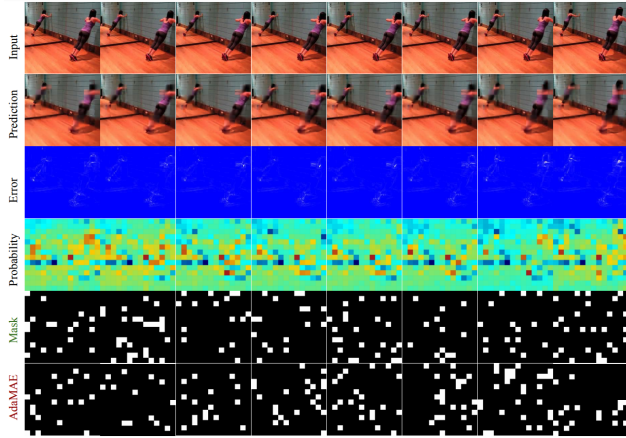


Figure 11. Sample Visualization of a UCF101 video with **adaptive sampling using TATS** with mask ratio $\rho = 0.9$. Compared with **AdaMAE [4]** masks.

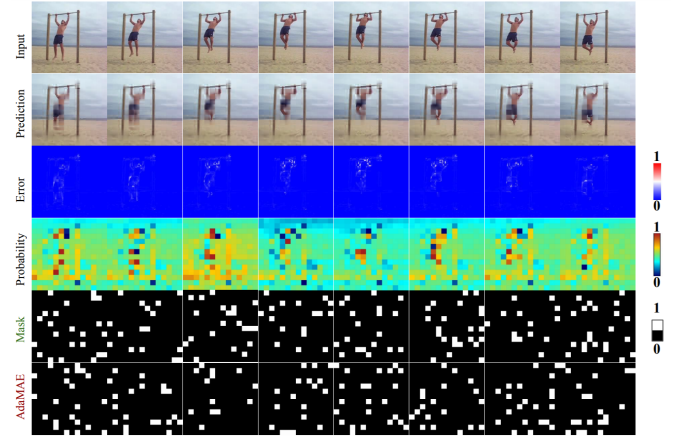


Figure 14. Sample Visualization of a HMDB51 video with **adaptive sampling using TATS** with mask ratio $\rho = 0.9$. Compared with **AdaMAE [4]** masks.

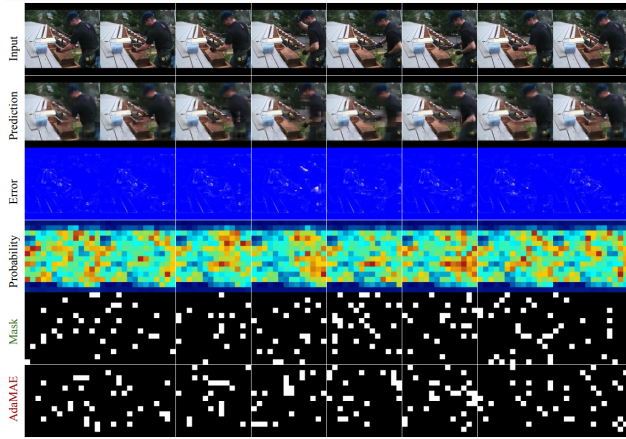


Figure 12. Sample Visualization of a UCF101 video with **adaptive sampling using TATS** with mask ratio $\rho = 0.85$. Compared with **AdaMAE [4]** masks.

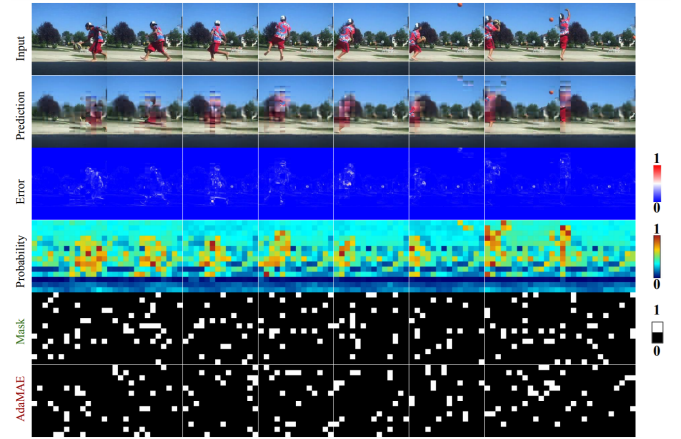


Figure 15. Sample Visualization of a HMDB51 video with **adaptive sampling using TATS** with mask ratio $\rho = 0.85$. Compared with **AdaMAE [4]** masks.